



Lodz University of Technology

SCIENTIFIC BULLETIN

PHYSICS

Vol. 39

LODZ 2018

LODZ UNIVERSITY OF TECHNOLOGY

SCIENTIFIC BULLETIN

No. 1224

PHYSICS

Vol. 39

LODZ 2018

ZESZYTY NAUKOWE POLITECHNIKI ŁÓDZKIEJ
SCIENTIFIC BULLETIN OF THE LODZ UNIVERSITY OF TECHNOLOGY
BULLETIN SCIENTIFIQUE
DE L'UNIVERSITÉ POLYTECHNIQUE DE LODZ
НАУЧНЫЕ ЗАПИСКИ
ЛОДЗИНСКОГО ПОЛИТЕХНИЧЕСКОГО УНИВЕРСИТЕТА
WISSENSCHAFTLICHE HEFTE
DER TECHNISCHEN UNIVERSITÄT IN LODZ

Editor of series: **Mariola Buczkowska, Ph.D., D.Sc., Eng.**

Subject Editor of series: **Assoc. Professor Jolanta Prywer, Ph.D., D.Sc., Eng.**

Printed version of the journal is the main version.

© Copyright by Politechnika Łódzka 2018

Adres Redakcji – Адрес Редакции – Editor's Office
Adresse de Redaction – Schriftleitungsadresse:

WYDAWNICTWO POLITECHNIKI ŁÓDZKIEJ

90-924 Łódź, ul. Wólczańska 223
tel. 42-631-20-87, 42-631-29-52
e-mail: zamowienia@info.p.lodz.pl
www.wydawnictwo.p.lodz.pl

ISSN 1505-1013
e-ISSN 2449-982X

doi:10.34658/physics.2018.39
<https://doi.org/10.34658/physics.2018.39>

<http://cybra.lodz.pl/publication/3923>

CONTENTS

Mariola Buczkowska – Flexoelectric torque in uniformly lying helix structures of chiral nematic liquid crystals.....5-12

Sylwester Kania, Barbara Kościelniak-Mucha, Janusz Kuliński, Piotr Słoma, Krzysztof Wojciechowski – Ab initio investigation of ethanol-tetracene interactions during adsorption.....13-25

Sylwester Kania, Janusz Kuliński, Dominik Sikorski – The origin of the interaction responsible for the difference of hole mobility of two derivatives of anthracene.....27-35

Julita Poborska, Dominika Dąbrówka, Maksymilian Chwirot, Rafał Ledzion, Marek Izdebski, Włodzimierz Kucharczyk – Frequency dependence of the Kerr constant in Nynas Nytro 3000 oil determined by the polarimetric method37-44

MARIOLA BUCZKOWSKA

Institute of Physics, Lodz University of Technology, ul. Wólczańska 219,
90-924 Łódź, Poland, e-mail: mariola.buczowska@p.lodz.pl

FLEXOELECTRIC TORQUE IN UNIFORMLY LYING HELIX STRUCTURES OF CHIRAL NEMATIC LIQUID CRYSTALS

Electric field induced deformations of chiral nematic liquid crystal layers were studied numerically. Uniformly lying helix structure of short pitch flexoelectric mixtures was considered. The electro-optic effect due to rotation of optical axis around the normal to the layer was simulated. The flexoelectric torque arising under the action of bias voltage and responsible for this rotation was calculated. It was found that the prevailing torque occurs in close vicinity of the boundary plates. Nonlinearity of superposition of splay and bend contributions to the total flexoelectric torque was found.

Keywords: chiral nematic, helical axis, flexoelectro-optic effect.

1. INTRODUCTION

Chiral nematic liquid crystals of pitch p shorter than visible light wavelength behave as uniaxial birefringent medium with optic axis parallel to the helix axis [1]. The twisted cholesteric structure within the layer confined between plane-parallel plates is incompatible with homeotropic boundary conditions. Therefore the subsurface regions are deformed by splay and bend. If the liquid crystal possesses flexoelectric properties then the deformation is accompanied by polarization of flexoelectric nature. An interesting linear electro-optic effect is possible under the action of the electric field of strength E applied perpendicular to the layer. The field interacts with the polarization and causes director rotation around the normal to the layer by a small angle Φ [1-3]. This effect results in change of orientation of the optical axis, which in this case is perpendicular to the twisted director (Fig. 1.). Interactions of dielectric nature are undesirable, because they induce a quadratic electro-optic effect and may lead to unwinding of the helical structure. Therefore the dielectric anisotropy of the

nematic should be zero or as small as possible. The rotation angle is approximately proportional to the electric field strength, according to the simplified formula

$$\Phi(E) = \frac{eEp}{2\pi k} \quad (1)$$

where e and k are the effective flexoelectric coefficient and the effective elastic constant, respectively [3]. The direction of deviation depends on the field sign. In the most favourable case, the angle Φ reaches $\pm 22.5^\circ$ which allows to switch between transmission 0 and 1 if the layer is placed between crossed polarizers [2]. The switching times are below 1 millisecond [4,5].

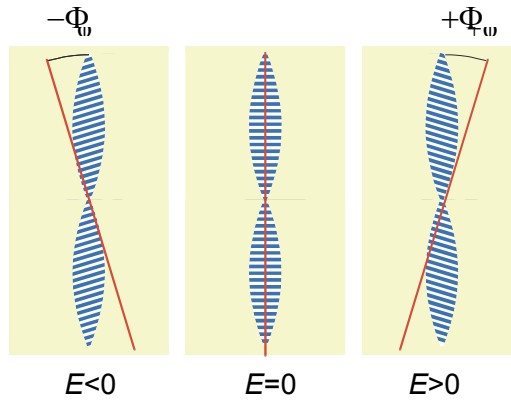


Fig. 1. Deviation of the optic axis under the action of electric field

2. ASSUMPTIONS AND METHOD

The aim of the present paper is to study the spatial distribution of flexoelectric torque responsible for rotation of the optical axis around the z axis. In particular it is interesting what is the role of flexoelectric coefficients e_{11} and e_{33} connected with splay and bend, respectively. For this purpose, the chiral nematic liquid crystal layer of thickness $d = 2 \mu\text{m}$ was taken into account. The layer was parallel to the xy plane of the coordinate system. It was placed between two electrodes positioned at $z = \pm d/2$. The helical axis was directed along the y axis. Director orientation was determined by the polar angle $\theta(y,z)$ made between the director and its projection on the xy plane, and by the azimuthal angle $\phi(z)$ between this projection and the x axis. Both angles as well as all other quantities were independent of the x coordinate. The azimuthal angle was assumed to be independent of y . The chirality of the nematic was determined by the intrinsic pitch, smaller than wavelength of visible light,

$p = 0.3 \mu\text{m}$. Homeotropic boundary conditions were assumed. The anchoring energy was determined by the polar and azimuthal anchoring strength coefficients, $W_0 = 10^{-4}$ and $W_\phi = 10^{-5} \text{Jm}^{-2}$, respectively ([6]). Dielectric anisotropy was assumed to be zero. Three sets of the flexoelectric coefficients were considered:

1. $e_{11} = 10 \text{ pC/m}$, $e_{33} = 0$,
2. $e_{11} = 0$, $e_{33} = -10 \text{ pC/m}$,
3. $e_{11} = 10 \text{ pC/m}$, $e_{33} = -10 \text{ pC/m}$.

Typical elastic constants were adopted: $k_{11} = 8 \text{ pN}$, $k_{22} = 4 \text{ pN}$, $k_{33} = 12 \text{ pN}$. The layer was subjected to voltage U ranging from 0 to 10 V. Nematic of high purity was assumed i.e. the presence of ions was neglected.

The deformation of the layer is caused by torque of flexoelectric origin (since $\Delta\varepsilon$ is assumed to be zero) which is given by vector product $\Gamma = \mathbf{P} \times \mathbf{E}$, where $\mathbf{P} = e_{11}(\mathbf{n} \cdot \nabla \mathbf{n}) - e_{33}(\mathbf{n} \times (\nabla \times \mathbf{n}))$ and $\mathbf{E} = -\nabla V$. In order to find the z -component of the torque responsible for rotation of the optical axis, $\Gamma_z = P_x E_y$, the director distribution over the cross section of the layer segment of width p was calculated. The minimization energy method described in detail in earlier papers was used for this purpose. The electric potential distribution $V(y, z)$ was also determined by resolving of the Poisson equation [7]. The calculations yielded the x -component of the flexoelectric polarization

$$P_x = e_{11} n_x \left(\frac{\partial n_y}{\partial y} + \frac{\partial n_z}{\partial z} \right) + e_{33} \left(n_y \frac{\partial n_x}{\partial y} + n_z \frac{\partial n_x}{\partial z} \right) \quad (2)$$

as well as the y -component of electric field strength

$$E_y = -\frac{\partial V}{\partial y} \quad (3)$$

which allowed to determine Γ_z .

3. RESULTS AND DISCUSSION

The typical deformation of the helical structure is presented in Fig. 2 by means of cylinders symbolizing the director. The azimuthal angle which measured the director rotation around the normal to the layer was found to adopt the same value in the prevailing part of the cross section with exception of thin subsurface regions. This value was taken as the rotation angle of the optic axis Φ . The director distribution is analogous to the pattern presented by Bouligand [3,8] i.e. it is composed of regions of splay and bend deformations. The spatial period of the deformed structure is equal to $p/2$ just like in the undisturbed chiral nematics in which the properties are repeated every half of pitch due to identity

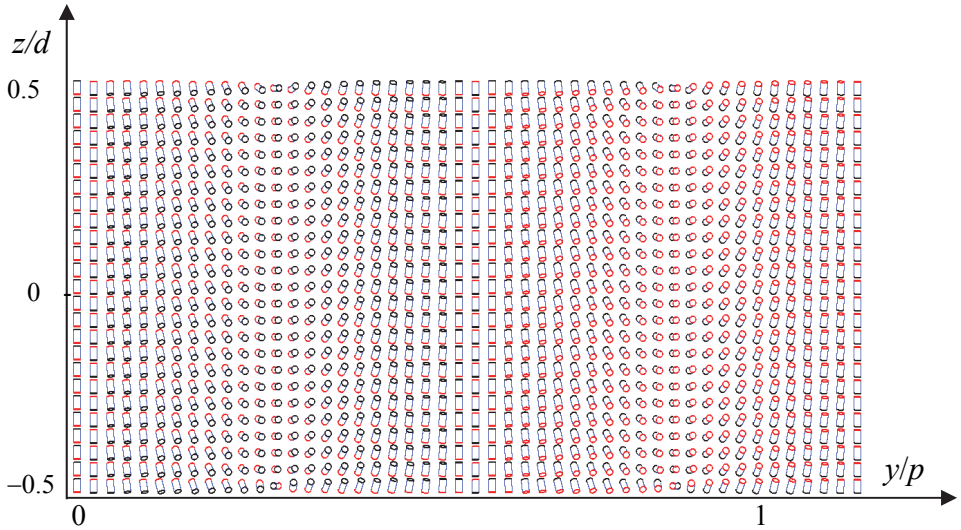


Fig. 2. Director distribution in the cross section of the layer along the pitch; $p = 0.3 \mu\text{m}$, $e_{11} = 10 \text{ pC/m}$, $e_{33} = -10 \text{ pC/m}$, $U = 12 \text{ V}$.

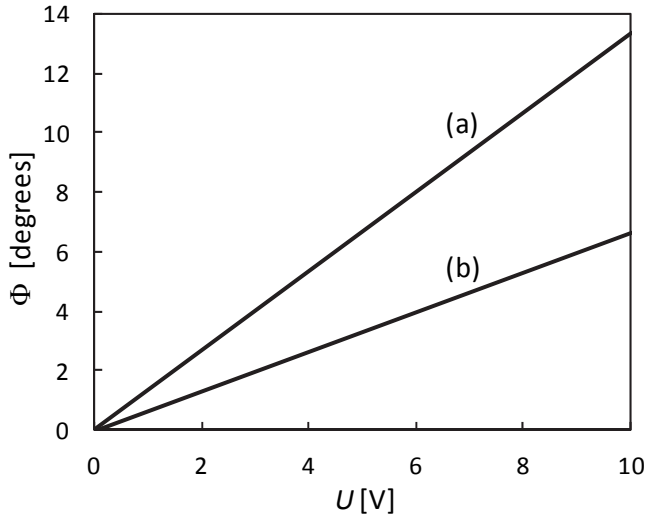


Fig. 3. Deviation angle Φ as a function of bias voltage; curve (a): $e_{11} = 10 \text{ pC/m}$ and $e_{33} = -10 \text{ pC/m}$; curve (b): $e_{11} = 10 \text{ pC/m}$ and $e_{33} = 0$ as well as $e_{11} = 0$ and $e_{33} = -10 \text{ pC/m}$; (both sets of flexoelectric coefficients give identical results).

$\mathbf{n} \equiv -\mathbf{n}$. The field induced deformations realized with the three mentioned sets of flexoelectric coefficients are qualitatively the same. In Fig. 3, the voltage dependencies of the angle Φ calculated for the three sets of flexoelectric coefficients are compared. It is evident that separate contributions of $e_{11} = 10$ pC/m and $e_{33} = -10$ pC/m to the electro-optic effect are identical due to equality $e_{11} = -e_{33}$ (curve b), whereas the simultaneous contributions of both coefficients lead to doubled rotation angles (curve a). It was also checked that rotation does not occur if $e_{11} = e_{33}$ i.e. if $e_{11} - e_{33}$ vanishes. The above statements are coherent with theoretical predictions that the angle Φ depends on difference of flexocoefficients, $e_{11} - e_{33}$, and not on their particular values [2].

The exemplary flexoelectric torques responsible for rotation of optical axis are illustrated in Figs. 4-6 as functions of y and z . The distributions are symmetrical with respect to $y = p/2$ i.e. $\Gamma_z(y) = \Gamma_z(p - y)$. This means that the spatial period of the torque is equal to p in contrary to the spatial period $p/2$ of the director distribution. Such property is due to the symmetries of the polarization and electric field components expressed by relations $P_x(y) = -P_x(p - y)$ and $E_x(y) = -E_x(p - y)$, respectively.

The flexoelectric torque counteracts the subsurface anchoring torque and the elastic torque in the bulk. It reaches the highest values at the boundary plates and in the regions where the director components n_x , n_y and n_z as well as their spatial derivatives have significant values. The equilibrium between the flexoelectric, elastic and anchoring torques can be achieved at high as well as at low values of flexoelectric torque and it can result in non-zero rotation angle Φ . Comparison of Figs. 4-6 with Fig. 2 shows that no torque is induced in the vicinity of $y/p = 0.25$ and $y/p = 0.75$. This is due to the fact that the deformation contains neither splay nor bend in those regions, therefore the flexoelectric polarization is zero. In the region surrounding $y/p = 0.5$, the n_x and n_y components are practically zero and the n_z component weakly depends on z therefore P_x (Eq. (2)) is negligible. The torque vanishes also at $y/p = 0$ and $y/p = 1$ for similar reasons.

The spatial distributions of torque over the cross section of the layer are rather complicated. The torque distributions vary with voltage. They arise as a result of self consistency between director field deformations producing flexoelectric polarization and interactions of the polarization with external electric field which also influence the director orientation.

In the case of $e_{11} = 10$ pC/m, $e_{33} = -10$ pC/m, (Fig. 4), both splay and bend give rise to the flexoelectric polarization and to the torque. The largest Γ_z values occur in the subsurface regions, in particular at $z = d/2$ and correspond to significant variations of director orientation. The small opposite torque occurs at

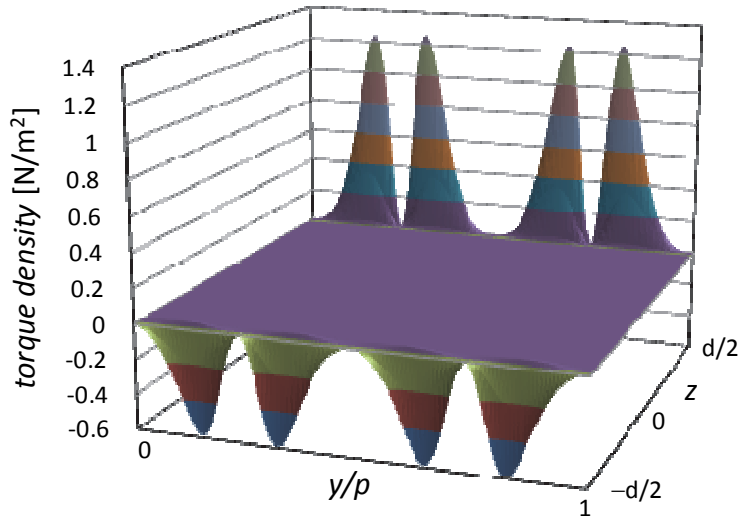


Fig. 4. Torque per unit volume as a function of position in the cross section of the layer; $p = 0.3 \mu\text{m}$, $e_{11} = 10 \text{ pC/m}$, $e_{33} = -10 \text{ pC/m}$, $U = 8 \text{ V}$.

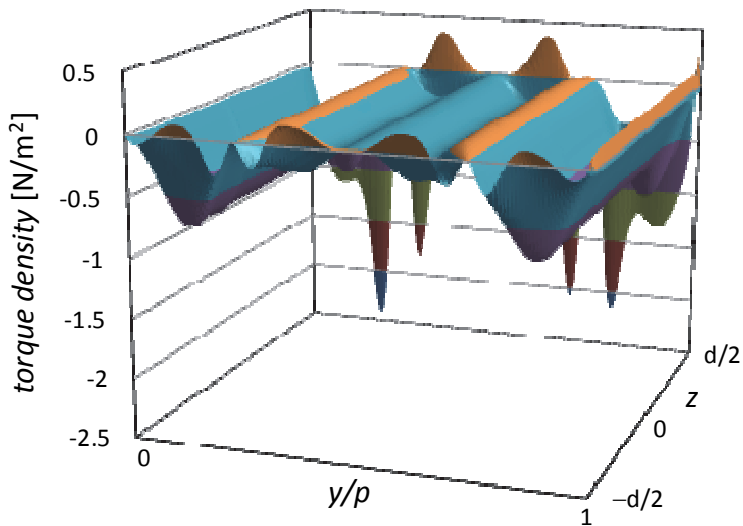


Fig. 5. Torque per unit volume as a function of position in the cross section of the layer; $p = 0.3 \mu\text{m}$, $e_{11} = 0 \text{ pC/m}$, $e_{33} = -10 \text{ pC/m}$, $U = 8 \text{ V}$.

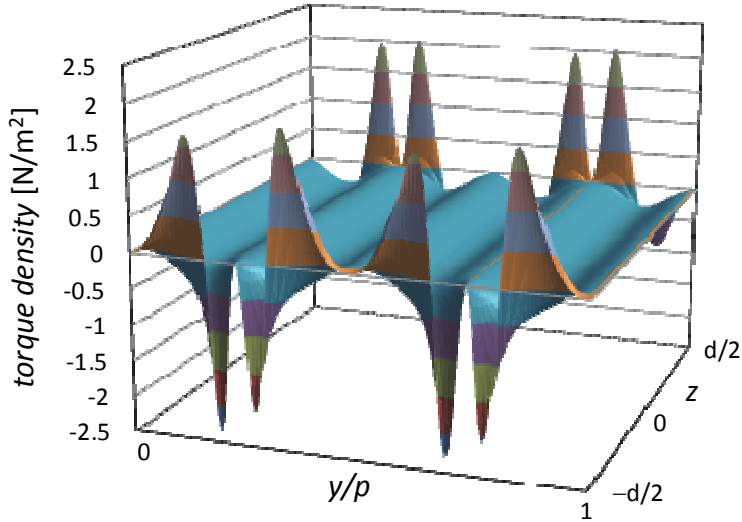


Fig. 6. Torque per unit volume as a function of position in the cross section of the layer; $p = 0.3 \mu\text{m}$, $e_{11} = 10 \text{ pC/m}$, $e_{33} = 0 \text{ pC/m}$, $U = 8 \text{ V}$.

$z = -d/2$ whereas the torques in prevailing part of the cross section are practically inessential. Much more complex distributions occur in the two other situations shown in Figs. 5 and 6. Significant torques arise not only in the vicinity of the boundary plates but also in the bulk of the layer. In particular, four regions of non-zero torques can be distinguished along the pitch. It is also evident that sum of the torque distributions occurring when either e_{11} or e_{33} are zero does not give the distribution arising when both flexoelectric coefficients do not vanish. This is an example of nonlinear superposition which is the pronounced manifestation of complexity of elastic, flexoelectric and surface interactions leading to equilibrium structures.

REFERENCES

- [1] Rudquist P., Buivydas M., Komitov L., Lagerwall S.T. 1994. Linear electrooptic effect based on flexoelectricity in a cholesteric with sign change of dielectric anisotropy. *J. Appl. Phys.* 76: 7778-7783.
- [2] Rudquist P., Carlsson T., Komitov L., Lagerwall S.T. 1997. The flexoelectro-optic effect in cholesterics. *Liq. Cryst.* 22: 445-449.
- [3] Rudquist P. 1997. On the flexoelectric effect in nematics. *Liq. Cryst.* 23: 503-510.

- [4] Kimura M., Naoto Endo N. 2016. Uniform lying helix of cholesteric liquid crystals aligned by means of slit coater method with electric treatment. IEICE Trans. Electron. E99-C: 1240-1243.
- [5] Varanytsia A., Chien L. 2015. Fast flexoelectric liquid crystal switching based on polymer-stabilized uniform lying helix. 2015 IEEE Photonics Conference (IPC). Reston, VA USA. pp. 38-44.
- [6] Derfel G, Buczkowska M. 2015. Macroscopic model formulae describing anisotropic anchoring of nematic liquid crystals on solid substrates. Sci. Bull. Techn. Univ. Lodz, Physics. 36: 5-12.
- [7] Buczkowska M., Derfel G. 2017. Spatially periodic deformations in planar and twisted flexoelectric nematic layers. Phys. Rev. E 95: 062705-1 - 062705-8.
- [8] Bouligand Y. 1969. Sur l'existence de „pseudomorphoses cholestériques” chez divers organismes vivants. J. Phys. Colloq. 30: C4-90-C4-103.

FLEXOELEKTRYCZNY MOMENT SIŁ W STRUKTURACH NEMATYKÓW CHIRALNYCH Z OSIĄ HELISY LEŻĄCĄ W PŁASZCZYŹNIE WARSTWY

Streszczenie

Zbadano numerycznie odkształcenia warstw nematyków chiralnych wywołane polem elektrycznym. Obliczenia dotyczyły nematyka o krótkim okresie struktury i właściwościach fleksoelektrycznych z osią helisy równoległą do płaszczyzny warstwy. Symulowano efekt elektrooptyczny polegający na obrocie osi optycznej warstwy wokół normalnej do płaszczyzny warstwy. Obliczono fleksoelektryczny moment sił powstający pod wpływem zewnętrznego napięcia i odpowiedzialny za ten obrót. Pokazano, że przeważający moment sił powstaje w pobliżu elektrod. Stwierdzono nieliniowy charakter superpozycji rozkładów momentów polegający na tym, że suma rozkładów momentów istniejących gdy $e_{11} = 0$ lub $e_{33} = 0$ różni się od rozkładu powstającego gdy oba współczynniki są różne od zera.

**SYLWESTER KANIA^{1,2}, BARBARA KOŚCIELNIAK-MUCHA²,
JANUSZ KULIŃSKI², PIOTR SŁOMA²,
KRZYSZTOF WOJCIECHOWSKI²**

¹ Institute of Physics, Lodz University of Technology, ul. Wólczańska 219,
90-924 Łódź, Poland

² Centre of Mathematics and Physics, Lodz University of Technology,
Al. Politechniki 11, 90-924 Łódź, Poland, e-mail: janusz.kulinski@p.lodz.pl

AB INITIO INVESTIGATION OF ETHANOL- TETRACENE INTERACTIONS DURING ADSORPTION

Ab initio calculations presented in this work are performed to investigate the geometry, interaction energy and bonding properties of binary complexes formed between neutral ethanol and tetracene molecules. Two different geometries were applied for the study. The interaction energies between molecules in the complex possess minimum at the distance of about 3.6 Å among oxygen atom in ethanol and the neighbouring carbon atom of tetracene skeleton.

Keywords: noncovalent interactions, adsorption energy, quantum chemistry calculations.

1. INTRODUCTION

It is well known that the interactions between molecules during adsorption are mainly an effect of a delicate balance between several weak noncovalent interactions [1]. Such interactions have been investigated extensively, both theoretically and experimentally in our previous works [2, 3, 4]. Kinetics of the change of the conductivity of the tetracene layer when exposed to ethanol vapour was considered as a phenomenon leading to an injection of the charge carriers. The thermodynamic force of this process was described as a consequence of the existence of two processes, the first being the two body interactions between the ethanol molecules in gas phase [4] and the second being two body interaction between ethanol molecule from the adsorption layer and tetracene molecule belonging to the solid film [3]. Our previous article [2] was devoted to the problem of the entanglement of the quantum states. Such

a problem appears during creation of the the dimer made of the ethanol and the tetracene molecules. The magnitude of the energy of the basis set superposition error (BSSE) was studied as a function of the distance d between ethanol and tetracene molecules calculated as the distance of the oxygen atom from ethanol molecule to the corner carbon atom at the side benzene ring of tetracene skeleton.

In this article, we review our previous results and report on new ones concerned with energy of interaction between ethanol and tetracene molecules. DFT (density functional theory) calculations with use Gaussian 09 package for interactions between neutral ethanol – tetracene molecules are presented. This is carried out to perform a comparative analysis of interactions between molecules of tetracene and ethanol for two similar geometries created by these molecules that form complex.

The dependence of the energy of the interaction of molecules with each other on the distance d is presented in this work.

2. EXPERIMENTAL APPROACHES

The basic technique for our adsorption studies of the ethanol – tetracene system is measurement of the dark current induced in the tetracene during activation by vaporization with ethanol molecules. The measuring cell of the “sandwich” type was a thin film made of tetracene supplied with Au-Al electrodes. Thin film of polycrystalline tetracene ($C_{18}H_{12}$) was prepared by evaporation in vacuum under a pressure of the order of 10^{-5} Torr on a glass substrate plate covered with Au electrode. The temperature of the substrate was about 300 K and the evaporation rate was varied within the range 20-30 Å/s. The thickness of the tetracene films were from 15 μm to 20 μm . The measuring cells were fixed in a vacuum chamber in a vacuum of approximately 10^{-5} Torr and were then subjected to the action of the activator vapour. The activator, C_2H_5OH , is characterized by high polarity with permanent dipole moment 1.7 D depending on the presence of OH group. This makes the sorption process possible. The measurements were performed at room temperature. The time dependence of the current flowing through the layer under an increasing concentration of active ethanol molecules in the vacuum chamber was recorded (see Fig. 1). The measurement device (Fig. 1) consists of a current source and an electronic $I-t$ recorder. The ethanol vapour pressure was 0.2 Torr. A single recording cycle of measuring data with multiple changing of the concentration of active ethanol molecules was of 1800 s. During a single cycle of recording of measurement data, the chamber was repeatedly supplied with new portion of active ethanol molecules. It was done when the current signal was saturated.

The measurements ended after rapid evacuation of the measuring system to high vacuum of 10^{-5} Torr. The electrical response measured in ethanol vapour showed a decrease of the resistance of the examined tetracene films. When the ethanol vapour flow was cut off and the measuring chamber was pumped to a high vacuum of 10^{-5} Torr, a rapid decrease in the current value to the level by one order greater than the initial value registered before ethanol was for the first time put into contact with a measured film.

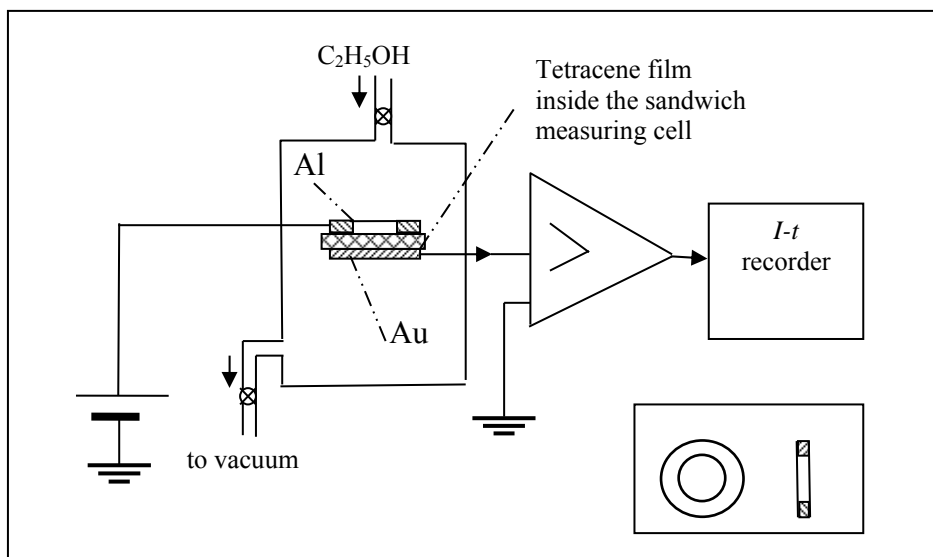


Fig. 1. Experimental set-up for activating the tetracene films and for recording the $I-t$ characteristics of the dark current induced by the activation process. Insert shows the construction of the upper aluminium electrode of the measuring cell.

3. COMPUTATIONAL DETAILS

The scan methodology allowed in the Gaussian 09 package was applied to illustrate the intermolecular interactions. The DFT calculations were made for neutral fragments. The B3LYP functional was chosen from a literature [5] as an effective tool for calculations of basic states of aromatic hydrocarbons. Ethanol-tetracene complex can be treated as a supermolecular system whose energy is obtained as a result of adding up the energy of the each individual molecular component. We have proved in our previous work [2] that basis set superposition error (BSSE) energy is of the order of magnitude of the ethanol-tetracene interactions. We must also bear in mind the fact that the magnitude

of van der Waals dispersive interactions are of the order of millielectronvolts. The BSSE arises because the orbitals of the neighbouring molecules will decrease the energy of the subject molecule even without transferring of the charge. Correction for the problem is supplied by the counterpoise method of Boys and Bernardi [6]. Such reasons and the complexity of calculations related to presence of heavy atoms as well as hydrogen make us to use B3LYP/6-311++G(d,p) with counterpoise correction. This *ab initio* technique gives a good agreement between the experiment and the calculated energies of orbitals for polycyclic hydrocarbons [7]. Employing calculations at such level of theory enabled us to realize the theoretical studies on the variability of the interaction caused when the ethanol molecule comes nearer in distance to the tetracene molecule.

The calculations were carried out for two cases: first, when the oxygen atom belonging to the ethanol molecule is moving in the distant plane parallel to the benzene of the tetracene skeleton and second one when the oxygen belonging to ethanol molecule is moving in the plane of tetracene skeleton.

3.1. Accuracy of the model

In order to model chemical systems accurately, one must account for their inherent quantum nature. The problem of exact energy decomposition of intermolecular interaction between two molecules is multifactorial. The total interaction energy E_T between two molecules can be described by an equation [8, 9]:

$$E_T = E_C + E_{excl} + E_p + E_{disp} \quad (1)$$

where E_C corresponds to the direct Coulomb interaction between two unperturbed charge distributions, E_{excl} denotes Pauli exclusion principle (exchange repulsion), E_p denotes the induction factor always attractive for electron pairs bonding, polarization and charge transfer, E_{disp} denotes always attractive intermolecular van der Waals interactions. For neutral fragments, the sum of E_C and E_{excl} is named as steric interactions [10, 11].

The complexity of the problem of quantum interactions between ethanol and tetracene molecules has been explored in an earlier works [2, 3]. It was shown that the problem of adsorption layer of ethanol at the solid layer of tetracene may be solved in the limits of the theory of an area law for entanglement from exponential decay of correlations [12] as a two body interaction problem. In practical quantum-chemical calculations we have studied such a two body interaction problem [2] with use DFT calculations with bases with a finite dimensions. Such calculations lead to a base superposition error (BSSE). This error of calculations was minimalized [2] thanks to the counterpoise correction (CP) proposed by Boys and Bernardi [6].

The evaluation of the magnitude of the error appears during DFT calculations made at temperature of 300 K was applied to confirm the validity of our numerical results.

The oxygen atom 31O of ethanol was placed initially at the distance $d = 3.43636 \text{ \AA}$ from carbon atom 20C of tetracene skeleton (Fig. 2). Optimization of the system was made with MP2/6-21g counterpoise calculation method. In Fig. 3 the dispersion of the calculations is presented. The uncertainty of the distance d we can estimate as $3 \cdot 10^{-5} \text{ \AA}$, of the bond length (20C-21C) as $4 \cdot 10^{-6} \text{ \AA}$, but the uncertainty of the total energy is of $6 \cdot 10^{-7} \text{ eV}$.

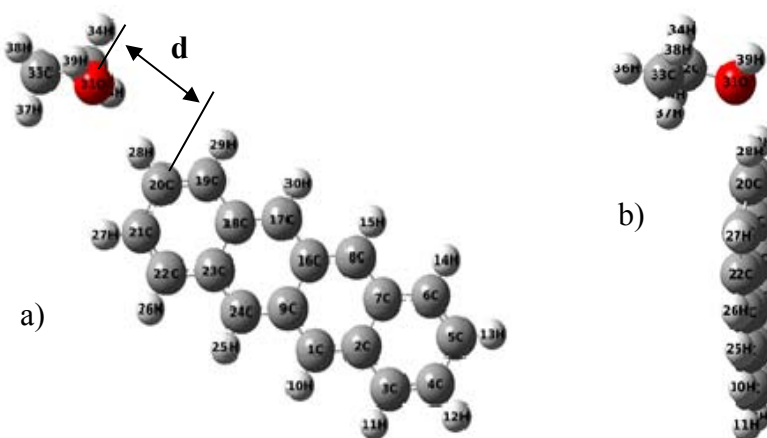


Fig. 2. Schematic images of the position of the ethanol and tetracene molecules determined in calculations by the distance d between oxygen atom 31O of ethanol with respect to the carbon atom 20C of tetracene skeleton: view of the entire complex, a) view of the position of the ethanol molecule in respect to the plane of tetracene skeleton b).

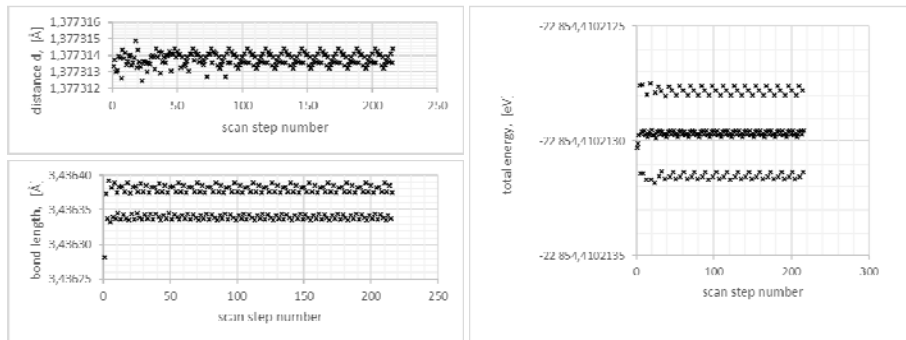


Fig. 3. Results of the DFT calculations of the equilibrium distance d of oxygen atom 31O of ethanol with respect to the carbon atom 20C in the plane of tetracene skeleton, bond length 20C-21C and total energy of a system.

4. RESULTS AND DISCUSSIONS

The quantum-chemical calculations with use of Gaussian 09 package were made with counterpoise correction of BSSE error with use of B3LYP/6-311++G(d,p) functional. In addition, the scan of the equilibrium structures along the distance d between 31O and 21C was performed. The transition states were calculated. Such transition states are difficult to observe experimentally because they are short-lived. They are not populated at equilibrium. Knowledge of such transition states allows understanding the mechanism of the possible path of charge transfer.

4.1. Simulation results

Proces of adsorption of ethanol on the tetracene surface is connected with decomposition of ethanol molecule at the tetracene and with transfer of electron from ethanol to tetracene during this process. The simulation results we want to present here can partially explain this phenomenon.

Fact that the tetracene molecule is more stable than ethanol is connected with the fact that the second excited level of ethanol molecule LUMO+1 is positive (see Table 1). It means that only one stable excitation level of -0.339 eV exists for electron in ethanol molecule, that is the LUMO orbital. Tetracene molecule in excited state LUMO+1 does not transmit electron easily

because of the negative energy of orbital in the range of -0.812 eV. Such a set of orbital energy values prefers transmission of electron from ethanol to tetracene when ethanol molecule approaches tetracene molecule while adsorption process is in progress.

Table 1

Frontier orbitals energies for ethanol and tetracene calculated by (DFT B3LYP/6-311++G(d,p))

Orbital	Ethanol Energy[eV]	Tetracene Energy [eV]
LUMO+1	+0.201	-0.812
LUMO	-0.339	-2.401
HOMO	-7.635	-5.141
HOMO-1	-9.228	-6.759

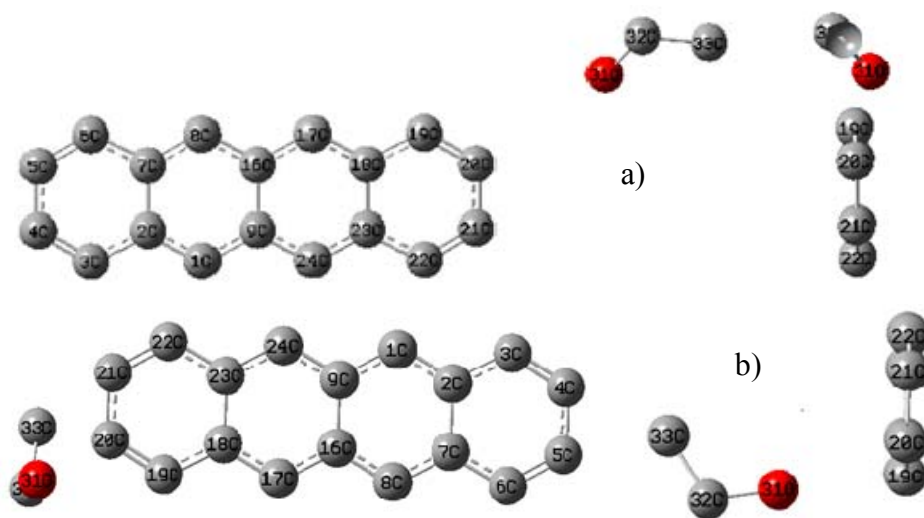


Fig. 4 The positions of two different orientations used to plot the HOMO LUMO levels in the Tables 2 and 3 (two views): ethanol in the tetracene plane a), ethanol distant from tetracene plane b).

The differences of the magnitude of energy of the same frontier orbitals for ethanol and tetracene (see Table 1) are responsible for observed shapes of HOMO and LUMO orbitals of the complex composed of interacting molecules as presented in figures placed in Table 2 and Table 3.

The geometry of two equilibrium ethanol positions relative to tetracene used for B3LYP/6-311++G(d,p) scan calculations with counterpoise correction is shown in the Fig 4.

The calculations of total energy also confirmed the existence of an adsorption layer built from ethanol molecules distant of about 3,6 Å from tetracene molecule. The observed minimum of total energy of the complex when ethanol is in tetracene plane at the distance of $d = 3,54$ Å (Fig. 5a.), and when ethanol is distant from tetracene plane at the distance $d = 3,58$ Å (Fig. 5b.).

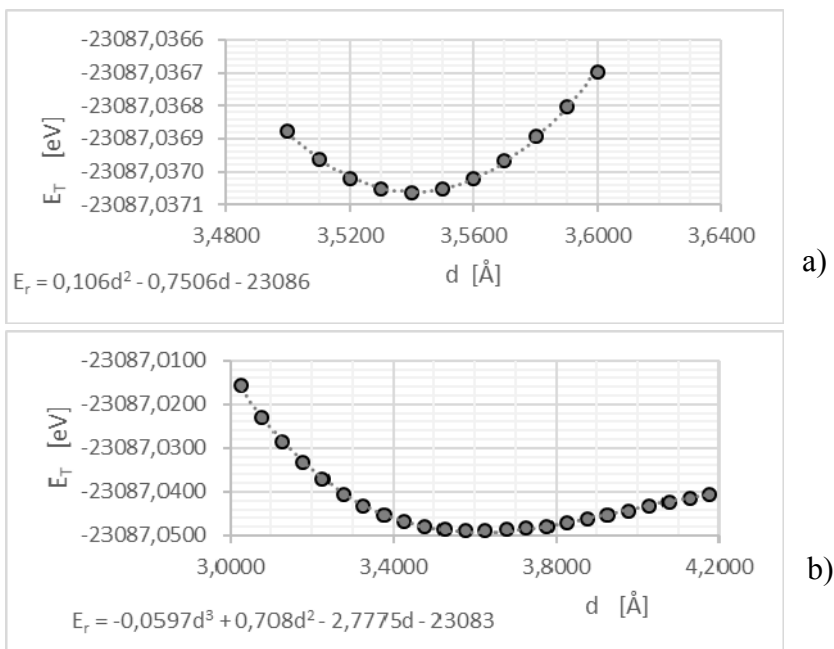


Fig. 5 Total energy of ethanol-tetracene complex of two different orientations used in DFT calculations: ethanol in the tetracene plane a), ethanol distant from tetracene plane b).

Table 2
Calculated energy and shapes of van der Waals LUMO orbitals (iso-value of 0.020) for both geometries of molecular complexes.


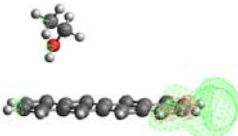

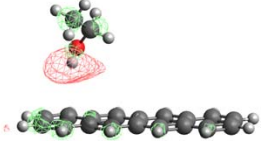

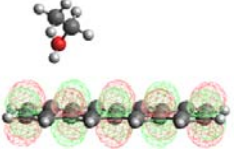

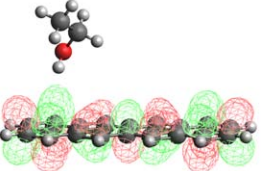

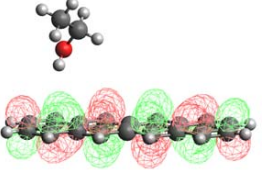
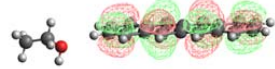
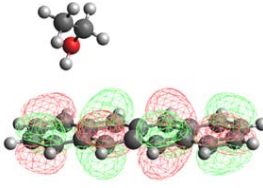
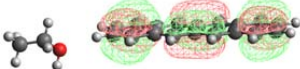
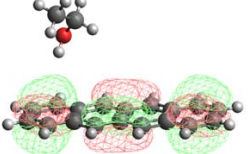

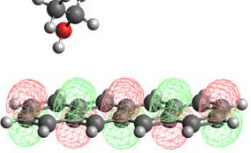

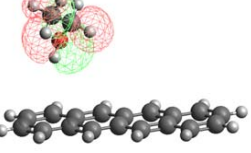
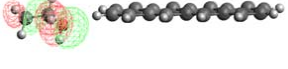
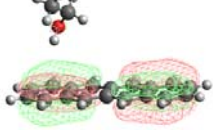
Orbital	Ethanol in tetracene plane		Ethanol distant from tetracene plane	
	Energy [eV]	complex	Energy [eV]	complex
LUMO+4	-0.101		-0,154	
LUMO+3	-0.473		-0.307	
LUMO+2	-0.669		-0.918	
LUMO+1	-0.707		-0.966	
LUMO	-2.305		-2.547	

Table 3
 Calculated energy and shapes of van der Waals HOMO orbitals (iso-value of 0,020) for both geometries of molecular complexes.

orbital	Ethanol in tetracene plane		Ethanol distant from tetracene plane	
	Energy [eV]	complex	Energy [eV]	complex
HOMO	-5.054		-5.297	
HOMO-1	-6.518		-6.772	
HOMO-2	-6.594		-6.846	
HOMO-3	-7.074		-7.455	
HOMO-4	-7.877		-7.927	

5. CONCLUSIONS

The energy dependence seen in Fig. 5 of the scan of total energy as the function of the distance d proved that a simplified van der Waals (vdW) dimer can be rather fluxional (without a well-defined geometric structure or equilibrium constant between the two molecules which form the complex) even at low temperatures, due to the very flat potential energies. The depth of the potential well ΔE_T does not exceed the value of kT at the calculated range of the variation of the distance d , i.e. in the order of 1 Å. The Boltzmann factor f determines the increase of the density of molecules in the potential well in comparison to the density in the outer space is determined as

$$f(\Delta E_T) = \frac{1}{\exp(-\Delta E_T / kT)} \quad (2)$$

where k is the Boltzmann constant $1.38 \cdot 10^{-23} \text{ JK}^{-1}$, T – Kelvin temperature used for calculations, $T = 300 \text{ K}$. Its value equal to $1/\exp(-1) = 2.73$ confirms the possibility of existence of the adsorption layer and tendency for ethanol to form clusters [13]. This adsorption layer appears as a result of interactions between neutral molecules. Such a process can explain only physisorption, i.e. the process without the exchange of electrons between interacting molecules. But our experiments have shown that conductivity of the tetracene layer increases in several orders of magnitude during vaporization of this tetracene layer with ethanol vapour. When analyzing this phenomenon it must be taken into account that the physical dimensions of ethanol molecule are so great that the diffusion of this molecule inside the tetracene layer is nearly impossible. Therefore, the only way for increase of the conduction of the tetracene layer, in that situation, is transfer of electrons in the contact interaction in the chemisorption layer or the desintegration of the ethanol molecule into smaller fragments.

The dynamic processes with exchange of electrons between ethanol and tetracene molecule, are different in two paths of movement described in this article. When ethanol moves in the tetracene plane (see Table 2) then the exchange of electrons is most probably when the transition LUMO+3 – LUMO+4 takes part. But when ethanol moves in the distant from tetracene plane but over the centre of the benzene ring of the tetracene skeleton than the exchange of electrons is most probably when the transition LUMO+2 – LUMO+3 takes part. The problem of how the molecule can be excited to the energy leading to above mentioned transitions needs further confirmation.

Acknowledgements

The results of quantum-mechanical calculations presented in this paper applied Gaussian-09 package implemented in the PLATON project infrastructure in the Computer Centre of the Lodz University of Technology.

REFERENCES

- [1] Karlický F., Otyepková E., Lo R., Pitoňák M., Jurecka P., Pykal M., Hobza P., Otyepka M. 2017. Adsorption of organic molecules to van der Waals materials: comparison of fluorographene and fluorographite with graphene. *J. Chem. Theory Comput.* 13: 1328-1340.
- [2] Kania S., Kościelniak-Mucha B., Kuliński J., Słoma P., Wojciechowski K. 2017. Sensitivity of tetracene layer. *Sci. Bull. Techn, Univ.Lodz, Physics*, 38: 45-51.
- [3] Kania S., Kuliński J. 2013. Adsorption of ethanol to thin layer of acenes as a process of interconnected networks. *Sci. Bull. Techn, Univ.Lodz, Physics*, 34: 27-34.
- [4] Kania S., Kuliński J. 2011. Absorbtion enhanced currents in thin layers of low dimension organics. *Sci. Bull. Techn. Univ. Lodz, Physics*, 32: 23-30.
- [5] Mallocci G., Cappellini G., Mulas G., Mattoni A. 2011. Electronic and optical properties of families of polycyclic aromatic hydrocarbons: a systematic (time-dependent) density functional theory study, *Chem. Physics* 384: 19-27.
- [6] Boys S.F., Bernardi F. 1970. The calculation of small molecular interactions by the differences of separate total energies. Some procedures with reduced errors. *Mol. Phys.* 19: 553-566.
- [7] Coropceanu V., Cornil J., da Silva Filho D.A., Olivier Y., Silbey R., Bredas J-L. 2007. Charge Transport in Organic Semiconductors, *Chem. Rev.* 107: 926-952.
- [8] Morokuma K., Kitaura K. 1981. Energy decomposition analysis of molecular interactions. [in:] *Chemical Applications of Atomic and Molecular Electrostatic Potentials*, ed. Politzer P., 215-242. New York: Springer Science and Business Media.
- [9] Chen W., Gordon M.S. 1996. Energy decomposition analyses for many-body interaction and applications to water complexes. *J. Phys. Chem.* 100:14316-14328.
- [10] Grimme S., Anthony J., Ehrlich S., Krieg H. 2010. A consistent and accurate ab initio parametrization of density functional dispersion correction (DFT-D) for the 94 elements H-Pu. *J. Chem. Phys.* 132: 154104-01-154104-19.
- [11] Grimme S., Ehrlich S., Goerigk L. 2011. Effect of the damping function in dispersion corrected density functional theory. *J. Comp. Chem.* 32: 1456-1465.
- [12] Brandão F.G.S.L., Horodecki M. 2015. Exponential decay of correlations implies area law. *Commun. Math. Phys.* 333: 761-798.
- [13] Karlický F., Otyepková E., Banás P., Lazar P., Kocman M., Otyepka M. 2015. Interplay between ethanol adsorption to high-energysites and clustering on graphene and graphite alters the measured isosteric adsorption enthalpies. *J. Phys. Chem. C* 119: 20535-20543.

BADANIE AB INITIO ODDZIAŁYWANIA ETANOL-TETRACEN PODCZAS ADSORPCJI

Streszczenie

Obliczenia kwantowo chemiczne potwierdziły istnienie warstwy adsorpcyjnej etanolu w odległości d ok. 3,6 Å od narożnego węgla w bocznym pierścieniu szkieletu tetracenu. Warstwa ta zapewnia jedynie zachodzenie procesu fizykosorpcji. Ponieważ badania doświadczalne wykazały wzrost skrośnego prądu płynącego przez warstwę tetracenu podczas procesu aktywacji tej warstwy w wyniku oddziaływania z parami etanolu, to musi tu jeszcze zachodzić proces związany z transferem elektronów. Proces taki jest procesem chemisorpcji. Uzyskane wartości energii orbitali LUMO dla kompleksu złożonego z cząsteczki tetracenu i etanolu wskazują że w przypadku, gdy wymiana elektronów zachodzi pomiędzy cząsteczką etanolu leżącą w płaszczyźnie szkieletu tetracenu a cząsteczką tetracenu to związane jest to z przejściem pomiędzy poziomami LUMO+3 i LUMO+4 kompleksu. Jeżeli jednak wymiana elektronu zachodzi podczas przemieszczanie się etanolu w płaszczyźnie odległej o ok. 3,3 Å od płaszczyzny szkieletu tetracenuowego ponad środkiem bocznego pierścienia benzenowego szkieletu tetracenu to wówczas wymiana elektronu pomiędzy cząsteczką etanolu a cząsteczką tetracenu zachodzi przy przejściu pomiędzy poziomami LUMO+2 i LUMO+3 kompleksu.

**SYLWESTER KANIA^{1,2}, JANUSZ KULIŃSKI²,
DOMINIK SIKORSKI³**

¹ Institute of Physics, Lodz University of Technology, ul. Wólczańska 219, 90-924, Łódź, Poland

² Centre of Mathematics and Physics, Lodz University of Technology, Al. Politechniki 11, 90-924 Łódź, Poland, janusz.kulinski@p.lodz.pl

³ Faculty of Material Technologies and Textile Design, Lodz University of Technology, ul. Żeromskiego 116, 90-924 Łódź, Poland

THE ORIGIN OF THE INTERACTION RESPONSIBLE FOR THE DIFFERENCE OF HOLE MOBILITY OF TWO DERIVATIVES OF ANTHRACENE

Hole mobility of the layers built from two anthracene derivatives differing in the substitution of the central benzene ring, i.e. anthrone substituted with only one keto group and anthraquinone substituted with two keto groups differs by one order of magnitude despite the fact that both have almost identical crystal structure. We ascribe this difference to existence of an additional intermolecular interaction arising in the layer of anthrone.

Keywords: anthrone, anthraquinone, DFT calculations, mobility.

1. INTRODUCTION

The process of generation and transfer of charge in solid organic materials cannot be described by just one theoretical model. This is due to the diversity of organic molecules and to the differences in their packing in the solid layer. In particular, among organic materials, active materials such as organic semiconductors built from the polycyclic molecules can be distinguished. They have an effect of aromaticity and constitute a quantum system, where the areas showing the effects of charge carriers localization and delocalization are bordering each other. The theory of hopping transport well describes charge carrier transport at room temperature for such an organic semiconductors.

Experimental determination of the microscopic properties of charge carrier transport needs the research on the electric transport in the layers of

materials creating similar crystal structure, but differing in only one element of structure of the molecules which compose the layer. Therefore this distinguished element of the structure of the molecule should be associated with this property of molecule which can significantly change the type of intermolecular interactions.

Potential of intermolecular electrostatic interactions is formed by sum of contributions derived from atomic charges, dipoles and the higher multipole moments which vanished by symmetry [1]. If the molecular crystal is formed only by the van der Waals interactions, the shortest intermolecular distances should be in the range as follows: C...H of 2.8 – 2.9 Å and C...C of 3.3 – 3.4 Å [2-3]. Therefore, at the distances of this range between adequate elements of the molecule, the contributions from atomic quadrupole moments can be neglected and for calculations of the crystalline electrostatic potential only atomic point charges and point dipoles should be used. In some molecular crystals the effect of the crystal structure exceeds the effect of presence of hydrogen bonding and is directed oppositely to it. In this case the total effect of crystalline electrostatic potential reduces the molecular dipole moment [2].

An interesting problem is the possibility of examination the properties of materials made of similar molecules but differentiating with one specific element of structure of molecule and simultaneously creating almost identical crystalline structures. Such experiment allows us to put the hypothesis that the variation of properties of such materials can be attributed to the element which differentiate the structure of molecules. Anthrone and anthraquinone are such a pair of molecules appropriate for comparison of properties in host solid state. Both of the mentioned above compounds crystallize in a similar crystal structure.

The parameters of nearly the same structures of anthraquinone, C₁₄H₈O₂ [4] and anthrone, C₁₄H₁₀O [5] are presented in Table 1.

Table 1.

The parameters of the crystal structures of anthraquinone [4] and anthrone [5] and their molecule dipole moment [6]

Compound	Space group	Lattice constant, [Å]	Lattice angle β [degree]	Dipole moment, [D]
Antraquinone (C ₁₄ H ₈ O ₂)	C _{2h} ⁵ (P2 ₁ /c)	a ₀ = 7.8684(5), b ₀ = 3.9634(3) c ₀ = 15.7839(13)	102.687(6)	0.6 (in benzene)
Anthrone (C ₁₄ H ₁₀ O)	C _{2h} ⁵ (P2 ₁ /c)	a ₀ = 7.8647(7) b ₀ = 3.9816(2), c ₀ = 15.813(1)	101.786(4)	3.66 (in benzene)

Our previous experiments have shown that there is a difference between mobility of anthraquinone and anthrone. Mobility of anthrone is of one order of magnitude greater than for anthraquinone layers. This difference is valid for polycrystalline, quasi-amorphous and amorphous layers for both considered compounds [7].

2. CALCULATIONS

The calculations were carried out with use of TD-DFT (time dependent – density functional theory) with GAUSSIAN 09 program [8]. The structures of anthraquinone and anthrone were optimized at B3LYP (Becke three parameter (exchange), Lee Yang, and Parr) method using 6-311+g(d,p) basis set. The structure was considered completely optimized when stationary point was located and was confirmed by absence of imaginary frequencies. Based on the optimized geometric structure, the HOMO, LUMO and band gap calculations were performed with the same level of theory at the ground state.

The optimized geometric structures with electrostatic potential map of the anthraquinone and anthrone molecules in the ground state are shown in Fig. 1. The distribution of the atom charges in the anthrone molecule indicates the presence of dipole moment marked in the Fig. 1a by an arrow.

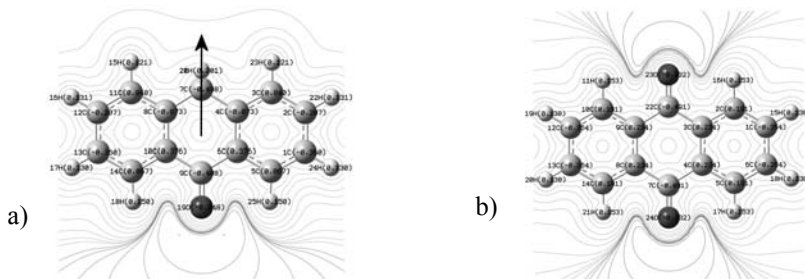


Fig. 1 The ground state of molecules of: a) anthrone (the arrow indicates the dipole moment) and b) anthraquinone. The electrostatic potential map is visualized and all of the atoms are signed with their symbols and their charge.

The bonds of the central ring of anthrone are single, i.e. 7C-8C, 7C-4C and 9C-10C, 9C-6C but all the others between carbons and carbon – oxygen are double. It is similar for the anthraquinone molecule, i.e. 22C-9C, 22C-3C

and 7C-8C, 7C-4C are single but all the others between carbons and carbon – oxygen are double. The symmetry of molecules causes that for anthrone the bonds lengths 7C-8C and 9C-10C are equal to bond lengths of 7C-4C and 9C-6C, respectively. For anthraquinone molecule we observe the same behaviour for bond lengths 22C-9C and 7C-8C in comparison to 22C-3C and 7C-4C.

Table 1
Bond lengths for anthrone and anthraquinone molecules in gas phase in comparison to the solid state.

anthrone			anthraquinone		
bond	gas phase	X-ray in solid phase [5]	bond	gas phase	X-ray in solid phase [4]
	[Å]	[Å]		[Å]	[Å]
19O – 9C	1.223	1.109	24O – 7C	1.220	1.224
9C – 6C	1.489	1.475	7C – 4C	1.492	1.478
6C – 4C	1.402	1.391	4C – 3C	1.406	1.372
4C – 7C	1.507	1.488	3C – 22C	1.492	1.478
7C – 20H	1.097		22C – 23O	1.220	1.224
6C – 5C	1.404	1.389	4C – 5C	1.398	1.391
5C – 1C	1.385	1.376	5C – 6C	1.390	1.372
1C – 2C	1.399	1.364	6C – 1C	1.398	1.410
2C – 3C	1.389	1.360	1C – 2C	1.390	1.372
3C – 4C	1.401	1.412	2C – 3C	1.398	1.391

3. DISCUSSION

The great difference about 6.4% in the length of the bonds among single bonds and double bounds existing between carbons in tetracene skeleton is observed for anthrone and anthraquinone. This difference takes place for molecules in gas phase and for molecules in solid phase.

The question arises if such a change of the single bond length between carbons in the middle rings for both considered molecules may be reflected in the different change of electronic properties of both molecules. The aromatic stabilization energy is the measure of aromaticity of the molecule and is correlated with the number of electrons contributing to aromaticity. Theory [9] suggests that interatomic exchange - correlation potential $V_{xc}(\Omega_A, \Omega_B)$, where Ω_A and Ω_B the interacting Quantum Atoms partitioning the energy of molecule into atomic (self) and interatomic (bond) parts of different topological subspaces, is to the first order approximation inversely proportional to the inter-nuclear distance R_{AB} between the nuclei of interacting atoms:

$$\frac{\delta(\Omega_A, \Omega_B)}{R_{AB}} = m \cdot V_{xc}(\Omega_A, \Omega_B) \quad (1)$$

m is an universal constant for any type of atom, and $\delta(\Omega_A, \Omega_B)$ is delocalization index used in the quantum theory of atoms in molecules (QTAM) equivalent to a covalent bond order [10]. The charges of carbon atoms are similar so $\delta(\Omega_A, \Omega_B)$ can be in analysis of single bonds considered as constant. The differences of R_{AB} for single bonds of anthrone and anthracene is less than 1%. Therefore we can assume that the change of aromatic stabilization energy for both examined molecules is nearly the same. This phenomenon is associated with a similar reduction of aromaticity of the central ring of both considered compounds. Therefore differences in charge transport properties between these compounds should not be sought in reduction of aromaticity of the molecule.

Therefore, we must look for another factor that has the potential to change the charge carrier transport which is observed in the solid layers.

The non-symmetrical substitution of anthracene molecule is realized with the origin of a large natural dipole moment of anthrone compared to the value of small dipole moment obtained while the symmetrical substitution is realized for anthraquinone. The increased mobility of charge carriers in anthrone layers should be related to the presence of the considerable value of dipole moment. The low mobility of charge carriers in anthraquinone is caused by a low value of dipole moment. This hypothesis could be built based on the obtained results described above.

To understand the role of dipole-dipole interactions occurring during charge transfer phenomena, it is necessary to analyze what are the sources of interactions. For this purpose it is convenient to analyse Hamiltonian describing such interactions.

The choice of the Hamiltonian in the situation described in this article is connected with the fact that nuclear dynamics is much slower than the dynamics of charge carriers and the fact that electronic coupling is weak. Hamiltonian for charge transport should be connected with static disorder, based on the assumption on the electronic density of states and on the hopping rates between localized states.

For low electron density materials one-electron Hamiltonian is convenient for presentation of the different kinds of charge carriers motion [11]:

$$H = H_0 + H_1 + H_2 + H_3 + H_4 \quad (2)$$

where:

$$\begin{aligned}
H_0 &= \sum_n \varepsilon \cdot a_n^+ a_n + \sum_\lambda \hbar \cdot \omega_\lambda \cdot \left(b_\lambda^+ b_\lambda + \frac{1}{2} \right), \\
H_1 &= \sum_n \sum_m J_{nm} \cdot a_n^+ a_m, \\
H_2 &= \sum_\lambda \sum_m g_{n\lambda}^2 \cdot \hbar \cdot \omega_\lambda \cdot a_n^+ a_m (b_\lambda + b_{-\lambda}^+), \\
H_3 &= \sum_n \sum_m \sum_{\substack{\lambda \\ n \neq m}} f_{nm\lambda}^2 \cdot \hbar \cdot \omega_\lambda \cdot a_n^+ a_m (b_\lambda + b_{-\lambda}^+), \\
H_4 &= \sum_n \delta \varepsilon_n \cdot a_n^+ a_n + \sum_n \sum_{\substack{m \\ n \neq m}} \delta J_{nm} \cdot a_n^+ a_n.
\end{aligned}$$

Hamiltonian H_0 represents the total energy of the system. It is assumed that the molecules and the lattice built by these molecules are in the excited state but without inter-interactions. Energy of the excited state of a molecule in the defined lattice node is described with node energy ε , its variations are described with $\delta\varepsilon_n$. The variation of ε is connected with non-phonon dispersion of energy states (diagonal elements H_{nn} of the Hamiltonian matrix). Non-diagonal elements δJ_{nm} ($n \neq m$, n, m – elements in the Hamiltonian matrix), represent the non-diagonal disorder of the force of interactions between two lattice nodes, but without presence of phonons (for example connected with disorder due to dipole-dipole orientation). a_n^+ , a_n are respectively the operators of creation and annihilation of excited electron with energy ε in the node n , and b_n^+ , b_n are respectively the operators of normal oscillations with energy $\hbar\omega_\lambda$ interact with electron in the state n and $g_{n\lambda}$ is non-dimensional coupling constant for this interaction. Transfer Hamiltonian H_1 describes electron transfer from node (n) to node (m) with overlapping energy J_{nm} . Terms H_2 and H_3 describe the impact of the lattice vibrations on the electron flow. The last H_4 is divided into two disorder terms, first one is responsible for statistic diagonal disorder and the second one for statistic non-diagonal disorder.

Dipole-dipole interactions energy between the dipole \vec{d}_{s_1} in the centre of the coordinate system having direction s_1 in the field originated from the network of point dipoles with directions s_n is shown below in the form of the sum of interactions with all other dipoles [12]:

$$\delta J_{1\alpha} = \frac{d^2}{2} \cdot \sum_{n=2}^{\infty} \left[\frac{\vec{s}_1 \circ \vec{s}_n}{|\vec{r}_{1n}|^3} - \frac{3 \cdot (\vec{s}_1 \circ \vec{r}_{1n}) \cdot (\vec{s}_n \circ \vec{r}_{1n})}{|\vec{r}_{1n}|^5} \right], \quad (3)$$

where r_{1n} is a position of n -th dipole, α -sign a manifold of the network of point dipoles.

This energy of dipole-dipole interaction may be an element for the second term in the Hamiltonian H_4 . In the case of anthraquinone, with the molecules with natural dipole moment measured in benzene of 0.6 D ($2.00 \cdot 10^{-30}$ Cm) [6], this energy is of the order of 10^{-5} - 10^{-6} eV, that is of three orders of magnitude less than the van der Waals potential energy (estimated in the range of 10^{-3} - $7 \cdot 10^{-2}$ eV), but anthrone molecules possess a significant natural dipole moment, when measured in benzene is of 3.66 D ($1.22 \cdot 10^{-29}$ Cm) [6] and in this case the energy of dipole-dipole interaction can be in the order of 10^{-2} - 10^{-3} eV. It means the value comparable to the van der Waals potential. These additional dipole-dipole energies present for anthrone structures can lead to broadening of the bands in the condensed form and to the enhanced overlapping of the wave functions for the charge carriers conducting via localized states.

3. CONCLUSIONS

In this article, we explicitly stated that for both described derivatives of anthracene, i.e. anthrone and anthraquinone, obtained as a substitution of the middle ring of tetracene skeleton with one or two ketone groups leads to the low almost identical (within 1% range) changes of the aromatic stabilization energy. At the same time, the determined change of bonds lengths between carbon atoms in the middle ring relative to analogous bond lengths for atoms in the side rings is of the value near 6.4%. This value is almost the same for both studied molecules. The above analysis of possible phenomena affecting the energy of interactions described by Hamiltonian terms indicated that the basic source of the difference in energy of interactions are dipole-dipole interactions. Therefore, the fact that mobility for polycrystalline, quasi-amorphous and amorphous layers of anthrone is of one order of magnitude greater than for anthraquinone layers can be attributed to the magnitude of the constant dipole moment of individual molecules. We believe that the only source of such differences of the mobility value of charge carriers for both considered compounds is the presence of the significant natural dipole moment in anthrone molecules in comparison to the anthraquinone molecules.

Acknowledgements

We are very much obliged for valuable discussion and contribution to the quantum calculations of dr. Piotr Słoma from Centre of Mathematics and Physics, Lodz University of Technology.

The calculations mentioned in this paper are performed using the PLATON project's infrastructure at Lodz University of Technology Computer Centre.

REFERENCES

- [1] Buckingham A.D., Fowler P.W. 1984. A model for the geometries of van der Waals complexes. *Can. J. Chem.* 63, 2018-2025.
- [2] Yatsenko A.V. 2003. Molecular crystals: the crystal field effect on molecular electronic structure. *J. Mol. Model.* 9, 207-216.
- [3] Weber G. 1981. The structure of a 2:1 host guest complex between p-nitroaniline and 18-crown-6. *Z. Naturforsch. B* 36, 896-897.
- [4] Fu Y. 1998. Temperature dependence of the rigid-body motion of anthraquinone. *B54*, 308-315.
- [5] Yap G.P.A., Wisner J.A. 1997. CSD Communication (Private Communication).
- [6] Landolt-Börnstein. 1971. *Zahlenwerte und Funktionen aus Naturwissenschaften und Technik*, Berlin: Springer Verlag.
- [7] Kania S. 2014. Hole drift mobility of anthrone and anthrachinone layers with different structures. *Sci. Bull. Techn. Univ. Lodz, Physics*, 35: 17-24.
- [8] Gaussian 09, Revision A.02. 2009. Frisch M.J., Trucks G.W., Schlegel H.B., Scuseria G.E., Robb M.A., Cheeseman J.R., Scalmani G., Barone V., Mennucci B., Petersson G.A., Nakatsuji H., Caricato M., Li X., Hratchian H.P., Izmaylov A.F., Bloino J., Zheng G., Sonnenberg J.L., Hada M., M. Ehara, Toyota K., Fukuda R., Hasegawa J., Ishida M., Nakajima T., Honda Y., Kitao O., Nakai H., Vreven T., Montgomery J. A., Peralta Jr., J.E., Ogliaro F., Bearpark M., Heyd J.J., Brothers E., Kudin K.N., Staroverov V.N., Kobayashi R., Normand J., Raghavachari K., Rendell A., Burant J.C., Iyengar S. S., Tomasi J., Cossi M., Rega N., Millam J. M., Klene M., Knox J.E., Cross J. B., Bakken V., Adamo C., Jaramillo J., Gomperts R., Stratmann R.E., Yazyev O., Austin A.J., Cammi R., Pomelli C., Ochterski J.W., Martin R.L., Morokuma K., Zakrzewski V.G., Voth G.A., Salvador P., Dannenberg J.J., Dapprich S., Daniels A.D., Farkas O., Foresman J.B., Ortiz J.V., Cioslowski J., and Fox D.J., Wallingford CT: Gaussian, Inc.

- [9] Badri Z., Foroutan-Nejad C. 2016. Unification of ground-state aromaticity criteria – structure, electron delocalization, and energy – in light of the quantum chemical topology *Phys. Chem. Chem. Phys.* 18: 11693-11699.
- [10] Pendás A.M., Blanco M.A., Francisco E. 2006. Chemical fragments in real space: definitions, properties, and energetic decompositions. *J. Comput. Chem.*, 28, 161-184.
- [11] Pope M., Swenberg C.E. 1982. *Electronic processes in organic crystals*, New York: Clarendon Press.
- [12] Kitaigorodskii A.J. 1973. *Molecular Crystals and Molecules*, New York: Acad. Press.

ŹRÓDŁO POWSTANIA ODDZIAŁYWAŃ ODPOWIEDZIALNYCH ZA RÓŻNICE RUCHLIWOŚCI DWU POCHODNYCH ANTRACENU

Streszczenie

Wykazano, w przypadku antronu i antrachinonu będących pochodnymi antracenu podstawionego w środkowym pierścieniu jedną lub dwiema grupami ketonowymi obserwuje się jedynie małe i prawie identyczne zmiany aromatycznej energii stabilizacji (w zakresie 1%). Oba rozpatrywane związki mają prawie identyczną strukturę krystaliczną. Jednakże ruchliwość dziur w antronie jest o jeden rząd wyższa niż w antrachinonie, niezależnie, czy jest badana w warstwach amorficznych, quasi-amorficznych czy też krystalicznych. Dlatego też jedynym źródłem obserwowanej doświadczalnie różnicy ruchliwości nośników ładunku może być obecność dużego momentu dipolowego cząsteczki antronu w porównaniu do małej wartości momentu dipolowego cząsteczki antrachinonu.

**JULITA POBORSKA, DOMINIKA DĄBRÓWKA,
MAKSYMILIAN CHWIROT, RAFAŁ LEDZION,
MAREK IZDEBSKI, WŁODZIMIERZ KUCHARCZYK**

Institute of Physics, Lodz University of Technology, ul. Wólczańska 219,
90-924 Łódź, Poland. e-mail: rafal.ledzion@p.lodz.pl

FREQUENCY DEPENDENCE OF THE KERR CONSTANT IN NYNAS NYTRO 3000 OIL DETERMINED BY THE POLARIMETRIC METHOD

A frequency dependence of the Kerr constant K in transformer oil Nynas Nytro 3000 within a frequency range 117-5017 Hz is determined. An averaged value $(2.30 \pm 0.03) \cdot 10^{-15} \text{ m/V}^2$ for K is obtained. The constant is found to be weakly frequency dependent and approaches its maximum $2.37 \cdot 10^{-15} \text{ m/V}^2$ at about 3000 Hz. The Kerr constant is of comparable value to that observed in other mineral oils employed previously in measurements of the quadratic electro-optic effect and the electrostriction in crystals.

Keywords: Kerr constant, Nynas Nytro 3000, electric field frequency.

1. INTRODUCTION

An electric field applied to isotropic media induces a change in their refractive indices and a rise of birefringence. It is known that isotropic media like liquids are centrosymmetric so all physical phenomena related to odd-order tensors are forbidden by the symmetry. Thus the lowest-order electro-optic effect that may be observed in liquids is the quadratic one. Higher-order effects are negligibly small and the quadratic is the only one that yields observable changes. In liquids this phenomenon is usually called as Kerr effect. Traditionally, the induced birefringence Δn is described in terms of Kerr constant K as

$$\Delta n = K \lambda E^2, \quad (1)$$

where λ is the light wavelength and E is the electric field strength [1-3]. The Kerr constant is in fact a tensor component thus K depends on directions of applied field and light propagation. The electric field induced changes may be described in a more general way using the following equation

$$B_{ij} = \varepsilon_0 (\varepsilon^{-1})_{ij} = \delta_{ij} n_i + g_{ijkl} E_k E_l, \quad (2)$$

where B_{ij} are the components of the impermeability tensor, ε^{-1} is the inverse of dielectric tensor, n_i are the principal refractive indices, g_{ijkl} the components of quadratic electro-optic tensor and E_k, E_l are electric field components. The form of tensor matrix shows that when the field is applied perpendicularly to the direction of light propagating in an isotropic liquid the electric field induced birefringence is [3-5]

$$\Delta n = \frac{1}{2} n_o^3 (g_{1111} - g_{1122}) E^2 = K \lambda E^2. \quad (3)$$

Our interest in studies of electro-optic properties of oils is related to the fact that in measurements of quadratic electro-optic coefficients in crystals we usually apply electric fields of strengths up to $1 \cdot 10^6$ V/m. The use of relatively high voltages imposes some precautions against investigated crystals. For example, the samples are often hygroscopic. To protect investigated crystals from moisture and reduce a probability of electric breakdown, the samples are immersed in liquids not solving the crystals. In interferometric experiments the use of a liquid with its refractive index close to the index of crystal suppresses light reflections at the sample faces. An immersing of the sample in the liquid allows also to ignore changes in the optical path resulting from electrostriction [6]. This is particularly important when the electrostriction of the sample is not precisely known. Moreover, an immersion liquid of appropriate viscosity suppresses sample vibrations causing substantial problems in precise interferometric measurements. All these reasons cause that the use of immersion liquids considerably improves the sensitivity of electro-optic measurements in crystals. Immersion liquids introduce an additional contribution to the light beam modulation which originates from a fringing electric field in the sample neighborhood and the Kerr effect of the liquid. Thus the knowledge of electro-optic properties of oils that may be used in investigations of the quadratic electro-optic effect in crystals is important. Mineral transformer oils have all desired properties and this is why we have been researching their properties for a long time (see, e.g. Refs [4, 5]). Moreover, the Kerr effect is interesting from the point of view of the relationship with aging processes of transformer oils [7]. In this work we study the frequency dependence of Kerr effect in a transformer oil Nynas Nytro 3000.

The intensity I of the light passing through a system composed of a Kerr cell and a quarter-wave plate placed between crossed polarizers is given by

$$I = \frac{1}{2} I_{\max} (1 - \cos \Gamma), \quad (4)$$

where Γ is the total phase difference introduced by the quarter-wave plate and the liquid in cell. If the oil is subjected to a sinusoidal field $E(t) = E_0 \sin(\Omega t)$, equation (4) takes the form

$$I = \frac{1}{2} I_{\max} \left[1 \pm \pi L K E_0^2 (1 - \cos 2\Omega t) \right], \quad (5)$$

where L is the path-length of light in the oil between electrodes and the signs “+” or “-” correspond to perpendicular or parallel azimuths, respectively, of the fast waves in the quarter-wave plate and in the oil. For typical values of the Kerr constant for oils the contribution of the Kerr effect to the DC component I^0 of the intensity I is negligible. Assuming that the voltage U at the output of photodetector is proportional to I , the depth of modulation at the second harmonic of applied field may be written as

$$m = \frac{I^{2\Omega}}{I^0} = \frac{U^{2\Omega}}{U^0} \approx \pi L K E_0^2. \quad (6)$$

In ref. [8] we showed that the sign of Kerr constant may be determined by a special variant of polarimetric technique. In this work only the magnitude of constant K is considered and the symbol K stands for the absolute value of Kerr constant. In Equation (6), $U^{2\Omega}$ is the amplitude of the second harmonic component and U^0 is the constant component in the total output voltage proportional to the emerging light intensity. Hence the Kerr constant is given by

$$K = \frac{m d^2}{\pi L U_m^2}, \quad (7)$$

where $U_m = E_0 d$ is the amplitude of the modulating voltage measured between electrodes at distance d .

2. EXPERIMENTAL SETUP

A diagram of the optical and electronic components used in our measurements is shown in Fig. 1. As a source of light a He-Ne laser with wavelength of 632.8 nm was used. A photodiode Thorlabs PDA36A-EC, DC voltmeter Keithley 2000 and a Lock-in voltmeter EG&G 7265DSP were

employed to measure components of the emerging light intensity. The electrodes attached to the cell served to apply the electric field perpendicular to the light direction. An internal generator of the Lock-in voltmeter with the amplifier and transformer was employed to provide the high voltage which was recorded by an AC voltmeter Fluke 45 with a probe Tektronix P6015A. The measurements were controlled by a PC computer. The same computer was used for the data acquisition. Parameters of electrodes were as follows: the length $L = (99 \pm 0.05)$ mm and the distance between them $d = (3 \pm 0.05)$ mm.

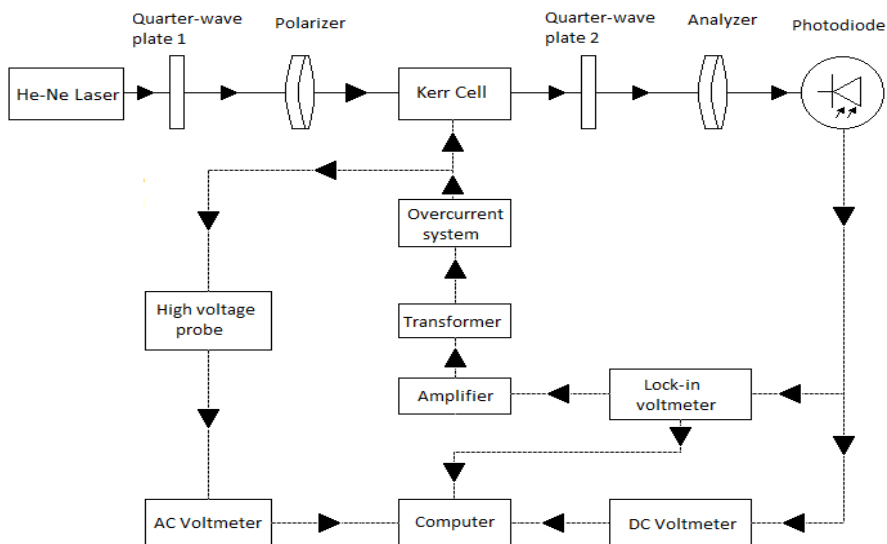


Fig. 1. Diagram of optical and electronic components used in measurements

3. NYNAS NYTRO 3000

The oil Nynas Nytro 3000 is manufactured by a Swedish company Nynas. It is a uninhibited mineral transformer oil without any additives to improve or change its properties. Its properties are typical for mineral transformer oils which makes it useful in the protection of crystal samples against moisture and reduction of the electric breakdown probability. Moreover, the moderate viscosity of the oil makes it useful in interferometric measurements.

Table 1

Some properties of the Nynas Nytro 3000 [9].

	temperature	average	maximum
density	20 °C	$0.870 \frac{\text{kg}}{\text{dm}^3}$	$0.895 \frac{\text{kg}}{\text{dm}^3}$
viscosity	40 °C	$9.5 \frac{\text{mm}^2}{\text{s}}$	$12.0 \frac{\text{mm}^2}{\text{s}}$
	-30 °C	$920.0 \frac{\text{mm}^2}{\text{s}}$	$1800.0 \frac{\text{mm}^2}{\text{s}}$

4. MEASUREMENTS AND RESULTS

Measurements of the Kerr constant were carried out in the frequency range 117 Hz-5017 Hz. For each frequency, the modulating voltage was changed within the range 500 V-2000 V with a step 100 V. Ten readings were taken for each voltage. In order to protect the results against imperfections of the quarter-wave plate, the readings were repeated for the plate rotated by 90°. The results obtained are illustrated in Fig. 2. It was found that values of the Kerr constant averaged over frequency and two 45° and 225° orientations is 2.188, while for 135° and 315° orientations it is 2.412, which means an offset of 0.224. Our measurements of the used quarter-wave plate along with numerical simulations of the measurement system with an imperfect quarter-wave plate based on the Jones calculus showed that the obtained results can be explained by a deviation of several degrees of the real value of the phase shift introduced by the plate from the ideal value of 90°. On the other hand, imperfections such as dichroism and the optical activity of the quarter-wave plate material have no significant effect. Our numerical simulations also showed that the inaccuracy of the phase difference in the quarter-wave plate leads to a systematic underestimation or overestimation of the K values obtained, depending on the orientation of the faster wave plane. Averaging the results obtained for orientations differing by 90° almost eliminates a systematic error, so there is no need to include it in estimating the uncertainty of the average value. The uncertainty obtained using the K constant values averaged over all orientations α_q for particular frequencies is $0.03 \cdot 10^{-15} \text{ m/V}^2$.

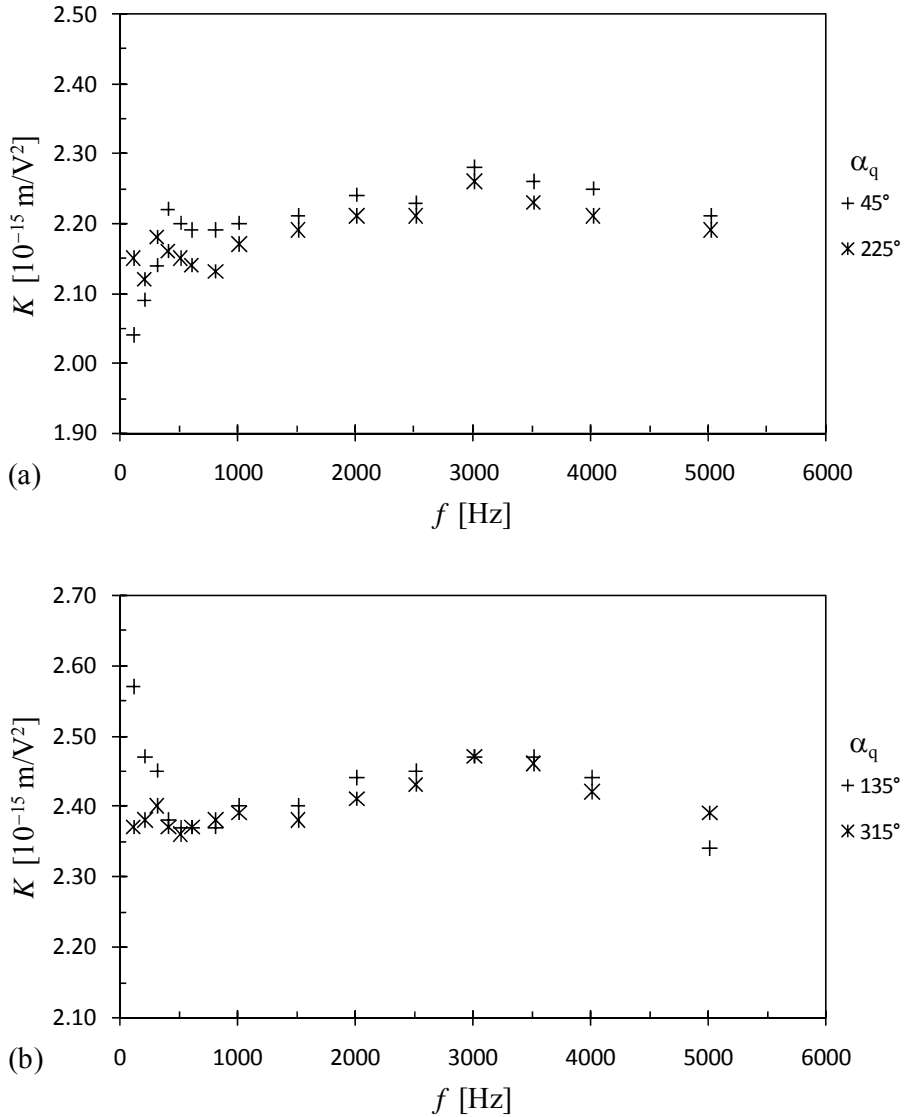


Fig. 2. An example of the dependence of the Kerr constant in Nynas Nytro 3000 oil on the modulating field frequency for different quarter-wave plate orientations α_q : (a) 45° and 225° , (b) 135° and 315° .

The results obtained indicate that the Kerr constant increases slightly up to the frequency of about 3000 Hz and then it starts to decrease. In our opinion, the

spread observed for frequencies below 500 Hz may result from effects arising from an orientational ordering of particles in oil [10].

Averaged values of the Kerr constant as related to the modulating field frequency are presented in Fig. 3.

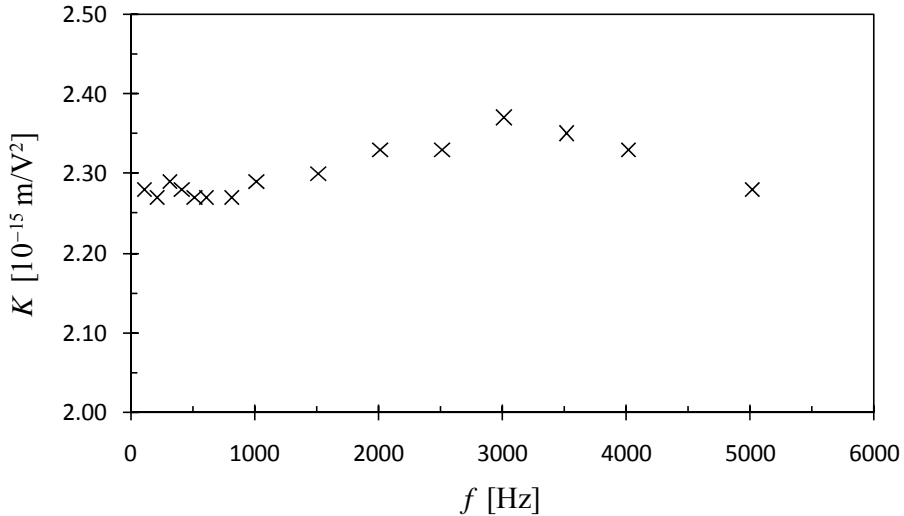


Fig. 3. Averaged values of the Kerr constant in the Nynas Nytro 3000 oil as related to the modulating field frequency.

5. CONCLUSIONS

The results obtained show that in the analyzed frequency range the Kerr constant in the mineral oil Nynas Nytro 3000 is weakly frequency dependent approaching its maximum $2.37 \cdot 10^{-15} \text{ m/V}^2$ at about 3000 Hz. Its average value was found to be equal $(2.30 \pm 0.03) \cdot 10^{-15} \text{ m/V}^2$. The constant K in the oil is of comparable value to that observed previously in other mineral oils which indicates that the oil may be useful as an immersion liquid in measurements of the quadratic electro-optic effect and electrostriction in crystals.

REFERENCES

- [1] Kerr J. 1875. A new relation between electricity and light: Dielectric media birefringent. *Philosophical Magazine* 50 (332): 337-348.
- [2] Born M., Wolf E. 1975. *Principles of Optics*, 5th edition, Oxford: Pergamon Press.

- [3] Ratajczyk F. 2000. Dwójłomność i polaryzacja optyczna, Wrocław: Oficyna Wydawnicza Politechniki Wrocławskiej.
- [4] Ledzion R., Bondarczuk K., Górski P., Kucharczyk W. 1999. Kerr constants of some mineral and silicone oils. *Quantum Electron.* 29: 739-741.
- [5] Górski P., Ledzion R., Sadowski M., Kucharczyk W. 2009. Effect of temperature on the refractive index and Kerr effect of the transformer oil NYNAS Nytro Taurus. *Sci. Bull. Techn. Univ. Lodz, Physics*, 30: 29-34.
- [6] Gunning M.J., Raab R.E., Kucharczyk W. 2001. Interferometric measurements of electrostrictive coefficients of KDP and ADP in Transmission. *Ferroelectric Letters* 28: 93-102
- [7] Kucharczyk W., Ledzion R., Górski P. 2014. The effect of aging of transformer oil on the magnitude and temperature dependence of its Kerr constant. *Przegląd elektrotechniczny (Electrical Rev.)* 12: 40-42.
- [8] Izdebski M., Ledzion R., Kucharczyk W. 2017. Application of polarimetric technique for determining the sign of quadratic electro-optic coefficients in crystals. *J. Opt. Soc. Amer. B* 34: 2281-2286.
- [9] <http://www.ms-oil.ch/media/files/002/0022002.pdf>
- [10] Izdebski M., Ledzion R. 2017. Kerr constant measurement technique for liquids exhibiting orientational ordering of molecules. *Optik* 140: 812-822.

CZĘSTOTLIWOŚCIOWA ZALEŻNOŚĆ STAŁEJ KERRA W OLEJU NYNAS NYTRO 3000 OKREŚLONA METODĄ POLARYMETRYCZNĄ

Streszczenie

W zakresie częstotliwości 117 Hz – 5017 Hz przeprowadzono pomiary stałej Kerra K oleju transformatorowego Nynas Nytro 3000. Otrzymana średnia wartość stałej wynosi $(2.30 \pm 0.03) \cdot 10^{-15} \text{ m/V}^2$ a w okolicach 3000 Hz osiąga ona maksymalną wartość $2.37 \cdot 10^{-15} \text{ m/V}^2$. Wyniki pokazują, że wielkość stałej Kerra w badanym oleju jest zbliżona do wartości obserwowanych w poprzednio badanych olejach więc może on być wykorzystany jako ciecz immersyjna w pomiarach współczynników kwadratowego efektu elektrooptycznego oraz elektrostrykcji w kryształach.

ISSN 1505-1013
e-ISSN 2449-982X
<http://cybra.lodz.pl/publication/3923>